Assessment of the Suitability of Ferrite Magnet Excited Synchronous Generators for Offshore Wind Turbines

Nurul Azim Bhuiyan
University of Strathclyde
nurul-azim-bhuiyan@strath.ac.uk

Alasdair McDonald
University of Strathclyde
alasdair.mcdonald@strath.ac.uk

Abstract:
In recent years the use of permanent magnets (PM) for wind turbine generators has increased significantly. The large price fluctuations encourage us to look at alternative PM materials. The main purpose of this paper is to assess the suitability or otherwise of a ferrite magnet excited synchronous generators for offshore wind turbines. Here, a generator design (for a 6 MW offshore turbine) using ferrite magnets is presented and compared with a generator using NdFeB magnets, in terms of capital costs, efficiency, and cost of energy. In order to do this a ferrite magnet generator is designed and compared to a design of a generator of the same rating that uses surface mounted NdFeB magnets.

Keywords: Cost of energy, permanent magnet (PM), neodymium, ferrite, wind turbine.

1. Introduction

Offshore wind turbines are increasingly using synchronous generators with permanent magnets manufactured using rare earth materials. These generators – whether they are high or low speed – tend to be more efficient than competing generator technologies such as the doubly fed induction or the field-wound synchronous generator. The lack of rotor copper losses means that these generators have flat, relatively high efficiency curves. This leads to higher energy yields, albeit at usually a higher cost. The onshore Cost of Energy calculation tends to push wind turbine designers to choose a cheaper induction machine. Offshore – where the non-turbine costs are so high – the Cost of Energy calculation puts a greater emphasis on maximising annual energy yield through maximising efficiency and availability. For something like the generator, which makes up only part of the capital cost but which involves all of the power output, it makes sense to choose highly efficient, reliable generators such as those using permanent magnets.

The most common material used in permanent magnet electrical machines is Neodymium - Iron - Boron (NdFeB). This class of material has a high maximum energy product (BH_{max} = 30-50MGOe) leading to compact machines with light generator rotors. The remanent flux density of these magnets can lead to airgap flux densities of the order of ~1T when the magnets are mounted onto the rotor surface.

During last few years, the price of NdFeB has increased and fluctuated significantly. China is the major producer of Nd with 97% of all mining currently in China. Export quotas are subject to strategic decisions, demand is high and growing (due to use in efficient electrical machines in new applications) and raw materials are subject to speculation [1]. The price of rare earth metals such as neodymium increased more than 350% from August 2009 to August 2011.This means that wind turbine manufacturers (who use permanent magnet generators) are faced with a significant cost uncertainty.

A number of researchers have started to explore alternative synchronous generator types that can deliver most of the benefits of these rare earth based permanent magnets. In the 1990s – before the cost of NdFeB allowed its economic use – designers would either opt for field wound synchronous machines or else use ferrite magnets [2]. In terms of availability and price stability, ferrite magnets can be a suitable alternative to NdFeB when mass (and inertia) of a generator rotor is of less importance [3]. These materials have a significantly lower maximum energy product (BH_{max} = 1-5 MGOe) and remanent flux density less than 0.4T. Some sample comparative data is given in Table 1. In order to produce higher flux densities in the airgap, machine designers must use some element of flux concentration so that a larger volume of ferrite magnet material (than the space generally used by a surface mounted magnet) can be used.

This paper builds on the work of Eriksson and Bernhoff [3] with an emphasis on a typical 6 MW

offshore wind turbine. In order to assess the suitability of ferrite magnets, two 6 MW wind turbine were designed: one with a surface mounted NdFeB rotor and another with a flux concentrating ferrite magnet rotor with same stator. The turbine in Hart *et al.* [4] is used as the basis for this.

This paper evaluates a design for a ferrite magnet generator for an offshore wind turbine. It looks at the potential downsides of using ferrite magnets such as increased generator mass, increased inertia and variation in loss mechanisms. To assess these, the main objectives are to model a 6MW wind turbine generator with the same stator but interchangeable rotors with different permanent magnet material. A ferrite magnet rotor is used to substitute a NdFeB rotor with the same airgap flux density. Some design optimisation is done to reduce the masses and inertia of the ferrite magnet generator rotor. Energy capture for the two generators is assessed, both from loss mechanisms within the generators and through variations in wind turbine rotor capture due to changes in rotational inertia. Finally a comparison of cost of energy for wind turbines with these two example generators is carried out.

Table 1. Example magnet properties for rare earth and ferrite magnet materials [5]

Magnetic Materials		
Magnet material	NdFeB	Ferrite
Grade	N40H	Y30
Remanence, min (T)	1.25	0.4
Normal Coercivity, min (kA/m)	923	240
Intrinsic Coercivity, min (kA/m)	1355	245
Density (kg/m^3)	7600	5000

In this section the case study wind turbine is defined, before generator modelling methods are outlined – these lead to loss calculations and generator costs. Next, the method for assessing the influence of rotational inertia and using this to estimate changes in annual energy production is described. Subsequent to that the cost of energy evaluation is defined.

2.1 Wind turbine data

This case study uses an offshore, 3 bladed, pitch regulated, variable speed wind turbine. The major ratings and assumptions are given in Table 2. When calculating steady power curves, it is assumed that the turbine rotor operates at maximum coefficient of performance below the rated wind speed. As a simplification for the analysis, it is assumed that for wind speeds above the rated, the blades are immediately pitched and power output is limited to 6MW and rotor speed is limited to 12rpm. The wind turbine cuts in at 3.5m/s and cuts out at 25 m/s. The turbine is placed at an offshore site with a mean wind speed of 9.6m/s, as defined using a Weibull distribution defined by the data in Table 2.

Table 2. Assumed characteristics for a simplified 6MW wind turbine and its wind resource.

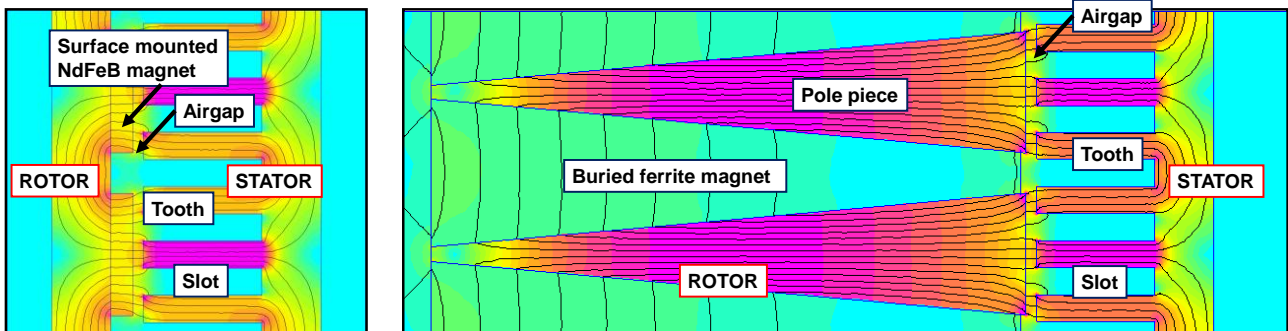| Wind Turbine Characteristics	
Rated grid power (MW)	6
Rotor Diameter (m)	145
Rated wind speed (m/s)	11
Rated speed (rpm)	11.6
Cut in wind speed (m/s)	3.5
Cut out wind speed (m/s)	25
Optimal tip speed ratio	8.3
Coefficient of performance at optimal tip speed ratio	0.48
Wind turbine availability (%) [6]	94
Wind turbine capital cost (*-cost of generator*) (×10^3 €)	6100
Site wind speed shape parameter	2.32
Site wind speed scale parameter (m/s)	10.8

2. Modelling Methods

Figure 1: Magnetostatic finite element analysis of surface mounted NdFeB generator (left) and flux concentrating ferrite generator (right). ■ 0T → ■ 1.5T . Software is FEMM [7]

2.2 Generator modelling

The method for calculating output power and common loss mechanisms are outlined below. Simplified ('linearised') sections of the two generator types are shown in Figure 1. The stators are identical, but the rotors are significantly different. This leads to some changes in the phasor diagrams. In order to calculate flux per pole, a lumped parameter magnetic circuit model is used. This is enhanced and verified using finite element software. The flux concentrating ferrite machine design was adapted to produce the same amount of flux crossing the airgap. The 2D models with end winding adaption are used to estimate inductance. Differences in generator rotor masses and moment of inertia were examined.

Table 3: Generator Material Characteristics

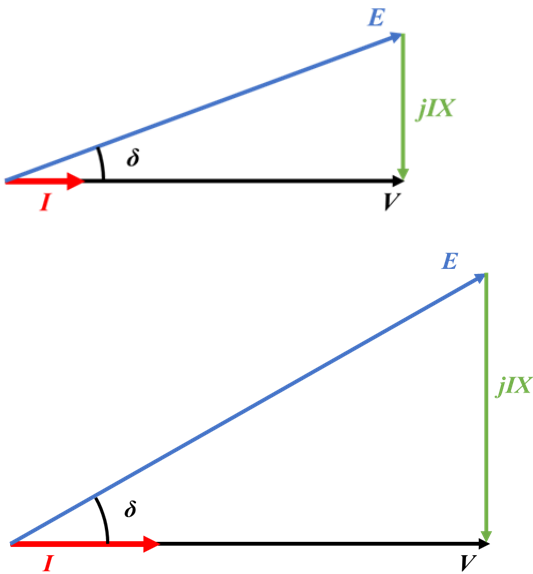| Generator Material Characteristics	
Slot filling factor k_{sfil}	0.6
Resistivity of copper at 120°C ρ_{cu} (µΩm)	0.024
Eddy-current losses in laminations at 1.5 T, 50 Hz P_{Feoe} (W/kg)	0.5
Hysteresis losses in laminations at 1.5 T, 50 Hz P_{Feoh} (W/kg)	2
Cost Modelling	
Power electronics cost (Euro/kW)	40
Lamination cost (Euro/kg)	3
Copper cost (Euro/kg)	15
Permanent magnet cost (Euro/kg)	60
Ferrite magnet cost (Euro/kg)	3
Rotor iron cost (Euro/kg)	2

Figure 2: Phasor diagram, when is generator operating at: (*a*, top) low wind speeds and (*b*, bottom) high wind speeds.

2.2.1 Power output and losses

In this paper it is assumed that the machines are run at unity power factor at all wind speeds. For the surface mounted machines, where $L_d=L_q$ and hence $X_d=X_q$. The following phasor diagrams can be used, if stator resistance is neglected. Figure 2(a) shows the generator operating at low wind speed and current. At higher wind speeds (e.g. Figure 2(b)) the induced emf, E, increases until pitch regulation starts and keeps the rotation speed constant. The current, I, is varied as shown in Figure 2, so that the correct power is produced at each wind speed. This implies that the load angle, δ, varies with wind speed up to rated wind speed.

The terminal voltage can be found with equation (1),

$$V = \sqrt{E^2 - (IX)^2} = E\cos\delta \qquad (1)$$

where X is the reactance.

In the case of the machines with a buried magnets there is significant saliency, i.e. $L_d \neq L_q$ [8]. In this case, the phasor diagram is shown in Figure 3 and the terminal voltage is found according to equation (2),

$$V = \sqrt{(E - I_d(X_d - X_q))^2 - (IX_q)^2}$$
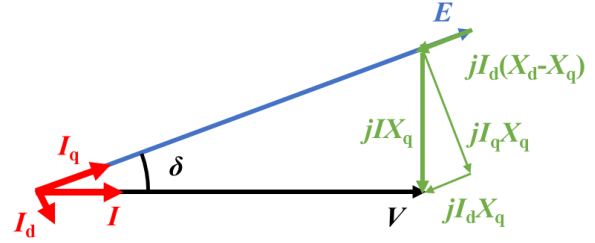$$= E\cos\delta - I_d(X_d - X_q)\cos\delta$$

Figure 3: Phasor diagram machine with buried magnet.

These equations can be solved iteratively to find the load angle for every wind speed if the relationship between wind speed and rotor speed and between wind speed and current are known. This allows the electrical output to be calculated,

$$P = 3IV. \qquad (3)$$

The copper losses can be calculated from currents and resistances. The phase resistance is given by:

$$R_s = \rho\frac{l_{cu}}{A_{cu}} \qquad (4)$$

where ρ is the resistivity of copper, A_{cu} is the cross-sectional area of the conductor and l_{cu} is the length of the conductor of the phase winding. The length of the conductor can be calculated as

$$l_{cu} = N_s(2l_s + 4\tau_p) . \qquad (5)$$

The cross-section area of conductor can be given as

$$A_{cu} = \frac{k_{sfil} A_{slot}}{N_{slot}} \quad (6)$$

where k_{sfil} is the slot fill factor, and

$$A_{slot} = w_s h_s \quad (7)$$

is the area of a slot and N_{slot} is the number of conductor per slot.

The magnetizing inductance of an AC machine is given by:

$$L_m = \frac{2\mu_0 l_s r_s (k_w N_s)^2}{p^2 g_{eff} \pi} \quad (8)$$

where l_s is the stack length in axial direction. r_s is the stator radius, N_s is the number of turns of the phase winding, k_w is the winding factor, p is the number of pole pairs and g_{eff} is the effective air gap. Leakage inductance can be calculated from [9]. The effective air gap of the surface mounted NdFeB machine can be written as,

$$g_{eff} = k_c \left(g + \frac{h_m}{\mu_{rm}} \right) \quad (9)$$

where k_c is the Carter factor of the stator slot. g is the mechanical air gap, h_m is the height of the magnet in the direction of magnetization. The Carter factor is given by

$$k_c = \frac{\tau_s}{\tau_s - g_1 \gamma} \quad (10)$$

where $g_1 = g + \frac{h_m}{\mu_{rm}}$,

$$\gamma = \frac{4}{\pi} \left(\frac{w_s}{2g_1} \arctan\left(\frac{w_s}{2g_1} \right) - \ln\sqrt{1 + \left(\frac{w_s}{2g_1} \right)^2} \right),$$

τ_s is the slot pitch and w_s is the slot width.

The specific iron losses (the iron losses per unit mass) are for the stator are calculated as

$$P_{Fe} = 2P_{Fe0h} \left(\frac{f_e}{f_0} \right) \left(\frac{\hat{B}_{Fe}}{\hat{B}_0} \right)^2 + 2P_{Fe0e} \left(\frac{f_e}{f_0} \right)^2 \left(\frac{\hat{B}_{Fe}}{\hat{B}_0} \right)^2 \quad (11)$$

where f_e is the frequency of the field in the iron, P_{Fe0h} is the hysteresis loss per unit mass at the given angular frequency f_0 and flux density B_0, and P_{Fe0e} is the eddy current loss per unit mass. To calculate the total iron losses, the iron losses in teeth and yokes are evaluated and added.

In order to calculate the annual electrical energy production of the turbine, it is necessary to also included losses in the power converter, turbine transformer and any cabling. These losses are evident in the difference between 'generator' and 'system' curves in later figures.

2.2.2 Airgap flux and induced emf

The no-load voltage induced by the flux density in a stator winding can be given as

$$E_p = \sqrt{2} k_w N_s \omega r_s l_s \widehat{B_g} \quad (12)$$

where ω is the mechanical angular speed of the rotor [10].

The fundamental flux density can be given as

$$\widehat{B_g} = B_g \frac{4}{\pi} \sin\left(\frac{\pi}{2} \frac{w_m}{\tau_p} \right) \quad (13)$$

where B_g is the amplitude of the quasi square air gap flux density, w_m is the magnet width and τ_p is the pole pitch. In a flux concentrating generator, the outer width of the pole w_{po} replaces the width of the magnet, w_m.

Lumped parameter magnetic circuits are used for both generator types to find the airgap flux density. The full magnetic circuits for one pole pair are shown in Figure 4.
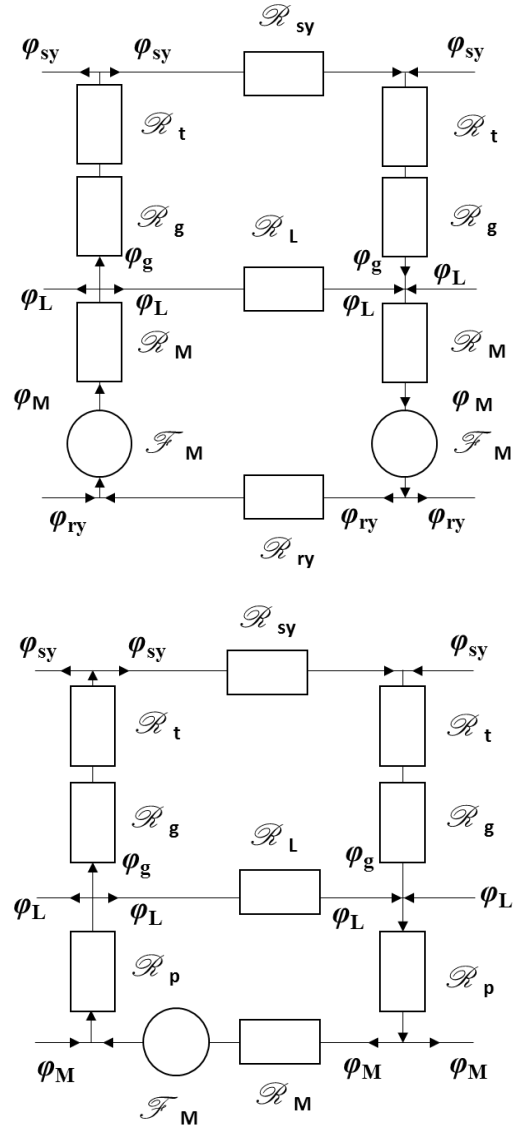

Figure 4: Magnetic circuits for modelling airgap flux per pole: (a, top) surface mounted magnet and (b, bottom) flux concentrating configuration.

2D finite element magnetostatic analysis was used to verify the airgap flux. This is shown for the two generators in Figure 1.

2.2.3 Masses and inertia

Masses of a material in generator can be calculated by multiplying the density of the material with its volume. Magnet mass can be calculated as

$$m_m = 2p\rho_m w_m h_m l_s \qquad (14)$$

where ρ_m is the density of magnet. To find out the cost of generator, the masses of iron and copper are also calculated and multiplied by the assumed cost per kilogram of the material.

Moment of inertia of rotating components with mass, m, at radius, r, on the rotor is given by:

$$I = \frac{1}{2}mr^2. \qquad (15)$$

Equation (15) can be used for the magnet, rotor iron and rotor structure (with correct masses and radii). The inertia of the rotating parts of the generator are used in Bladed model to compare the energy capture of generator with different inertia, as described in Section 2.3.

2.2.4 Ferrite magnet generator: magnet mass minimisation

With a fixed pole width and number of pole pairs, the flux concentrating magnet geometry can be optimised to minimise magnet mass while achieving the same fundamental flux density as the surface mounted magnet machine. Increasing the magnet width at the inner radius ($w_{m,i}$) leads to the angle θ increasing (Figure 5). This variation, accompanied with changing in the magnet height (h_m) allows the magnet mass to be minimised.
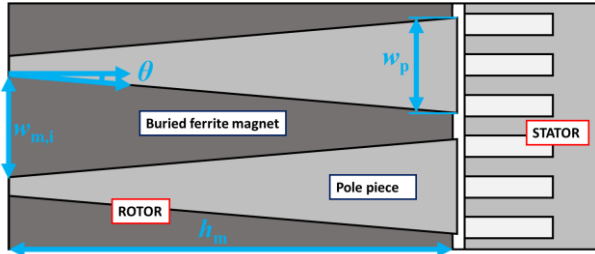

Figure 5: Schematic diagram for ferrite magnet rotor with angular pole

To further minimise magnet mass, contour plots of magnet mass and airgap flux density from surface mounted NdFeB and flux concentrating ferrite rotors are plotted against different magnet widths and heights.

2.3 Calculation of annual energy production

The assumed wind turbine mechanical power curve is shown in Figure 6. Each generator has the same rated torque but there are differences in efficiency due to the varying current loading (caused by the variance in inductance) as described in Section 2.2.1. This leads to different losses at each wind speed and hence the

generator efficiency curves in presented in Section 3. To calculate the baseline Annual Energy Production, first the Electrical Power, $P_{\text{Electrical}}(v)$ at each wind speed, v is given by,

$$P_{\text{Electrical}}(v) = P_{\text{Mechanical}}(v)\eta(v) \qquad (16)$$

where $P_{\text{Mechanical}}(v)$ is the power from the wind turbine rotor and $\eta(v)$ is the electrical system efficiency.

The assumed wind speed Weibull probability distribution is shown in Figure 7 (with an assumed shape parameter, k= 2.32 and a scale parameter, C = 10.8 m/s).

Equation (17) gives the probability of a given range of wind speeds ($A < v \leq B$),

$$p(A < v \leq B) = Q(v > A) - Q(v > B)$$
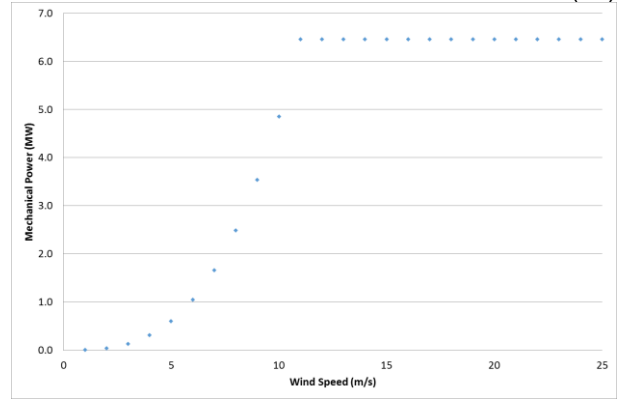$$= e^{-(A/c)^k} - e^{-(B/c)^k}$$

$$(17)$$

Figure 6: Mechanical power vs. wind speed for the assumed wind turbine.
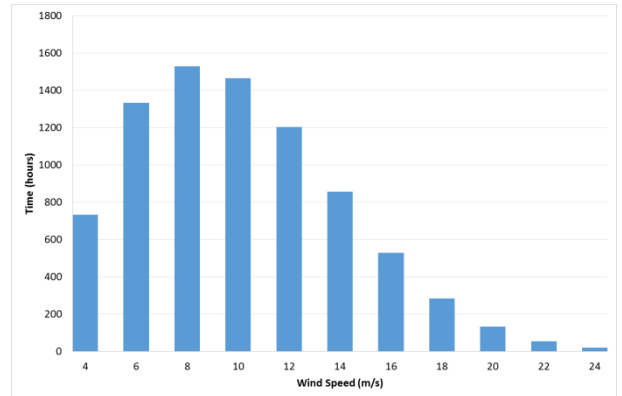

Figure 7: Weibull probability distribution

To calculate the Annual Energy produced at each wind speed range in a year, equation (18) gives,

$$E(A < v \leq B) \cong 365 \times 24$$
$$\times p(A < v \leq B)P_{\text{Electrical}}(\bar{v} = x)$$

$$(18)$$

where E is the Annual Energy for the range of wind speed and x is the average wind speed of that range.

Repeating this for a number of wind speed ranges between cut in and cut out wind speeds gives the Annual Yield curves in Section 3. The integral of such a curve will give the Annual Energy Production, with units of Wh.

2.4 Estimating the influence of varying inertia

In order to assess the influence of varying generator rotor inertia, a number of Power Production simulations were carried out using Bladed[11]. Wind speed time series were created with turbulence at different average wind speeds. (Figure 8, shows one sample when the mean wind speed is 12m/s).
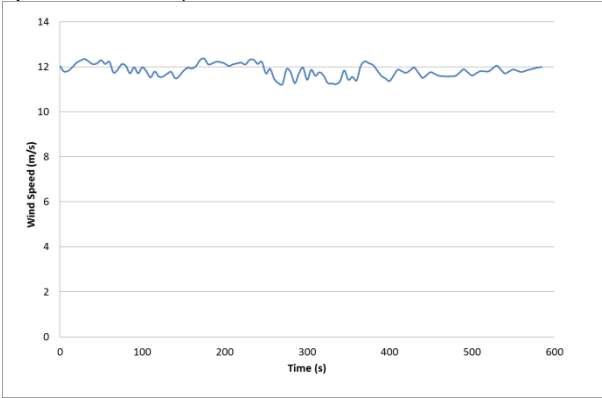

Figure 8: Sample wind speed time series, with $\bar{v}$ = 12m/s

Two wind turbine models were created, identical apart from the generator rotor inertia. Each wind speed time series was run to evaluate the different energy capture of these two turbine models. If the energy capture during the sample time series for the baseline wind turbine is $E_{\text{sample},1}(\bar{v} = x)$, then the energy capture for the turbine with the modified generator rotor for the same wind speed time series is $E_{\text{sample},2}(\bar{v} = x)$. This can be repeated for different average wind speeds. For this analysis, it is assumed that equation (19) holds and that,

$$\left(\frac{E_2}{E_1}\right)_{\bar{v}=x} = \frac{E_{\text{sample},2}(\bar{v}=x)}{E_{\text{sample},1}(\bar{v}=x)} . \tag{19}$$

Equation (19) can be adapted for the new generator rotor inertia,

$$E(A < v \leq B) \cong 365 \times 24 \times p(A < v \leq B)P_{\text{Electrical}} \ (\bar{v} = x)\left(\frac{E_2}{E_1}\right)_{\bar{v}=x}$$

and subsequently a new, modified Annual Energy Production can be calculated.

2.5 Cost of energy

The Cost of Energy (COE) can be calculated by,

$$COE = \frac{(FCR \times ICC + AOM)}{AEP} \tag{21}$$

where FCR is the fixed charge rate, ICC is the initial capital cost of the turbine, AOM is the annual operation and maintenance and AEP is the annual energy production.

Here ICC and AOM are calculated according to [4] and AEP is calculated using the method described in Sections 2.2-2.4.

3 Results

3.1 Generator modelling

The airgap flux density of the two generator rotors were modelled using FEMM software. Contour plots were used to reduce magnet mass. Figure 9 shows the effect of magnet height and magnet width on the airgap flux density and magnet mass for the two machines. Figure 9(a) shows how the falling marginal improvement in airgap flux density as magnet height increases and how for a given magnet height, airgap flux per pole is very nearly proportional to width of the magnet. Figure 9(b) gives the flux concentrating magnet rotor. Here the mass of magnets for the same airgap flux density is far greater. For a fixed pole pitch, when the magnet gets wider the pole width gets smaller, exaggerating the increase in airgap flux density (albeit over a narrow pole).
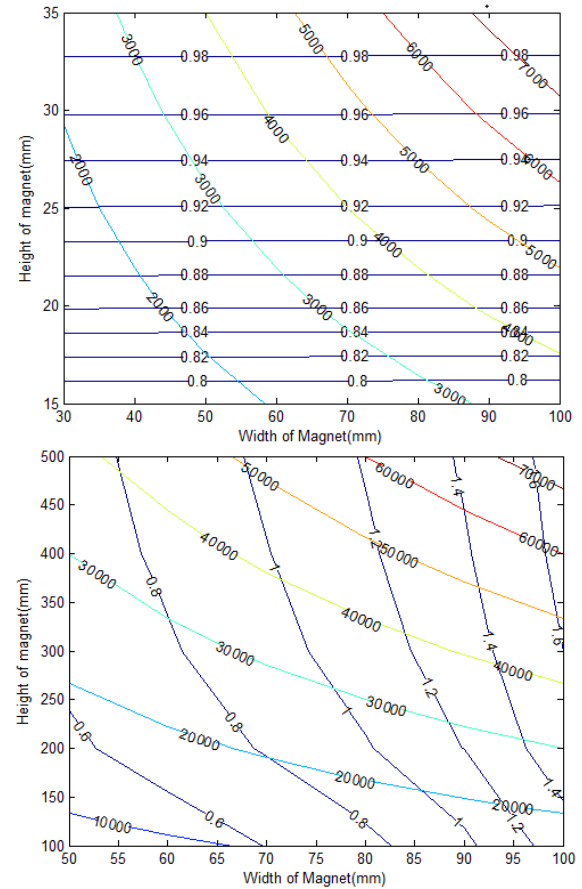

Figure 9: Contour plots of airgap flux density (blue, labelled in T) and magnet mass (multi-coloured, labelled in kg).(a, *top*) surface mounted NdFeB rotor and (b, *bottom*) flux concentrating ferrite magnet rotor.

To check that similar air gap flux density waveforms are produced, the simulated waveforms produced from the finite element modelling (Figure 1) were passed through a Fast Fourier Transform to identify the spatial harmonics. Figure 10 (a) and (b) show that the amplitude of the fundamental airgap flux density ($\widehat{B_g}$ = 0.91T) is the same and there are minor differences in the 3rd and 5th harmonics; overall it can be surmised that the two rotors are able to produce the same fundamental induced EMF.
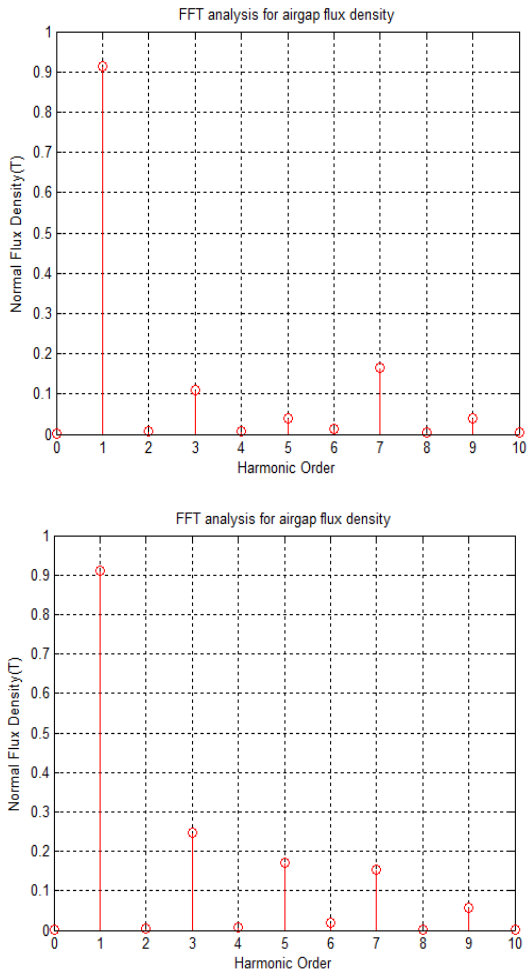

Figure 10: FFT analysis of airgap flux density waveform for (a, *top*) surface mounted NdFeB generator and (b, *bottom*) flux concentrating ferrite generator.

As shown in Section 2.2.4., the flux concentrating buried magnet rotor can be further optimised by increasing the magnet width at inner radius and altering the magnet height to get the same airgap flux density with surface mounted NdFeB rotor. Figure 11 shows that for a constant magnet mass (37,600kg), higher airgap flux densities as the angle increases. The maximum value of the angle is $\theta_{\max}$ =6.2° which occurs when $w_{\mathrm{m,i}} = \tau_\mathrm{p}$.

It also possible to produce the same airgap flux density (as the surface mounted NdFeB) by reduce

mass by increasing the angle θ and decreasing magnet height. Figure 12 shows a line of constant airgap flux density ($\widehat{B_g}$=0.91T) and how the magnet mass can be minimized.

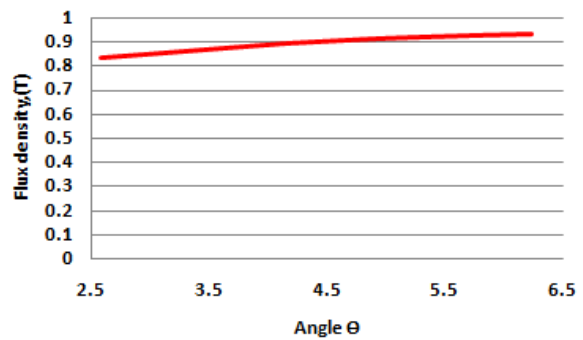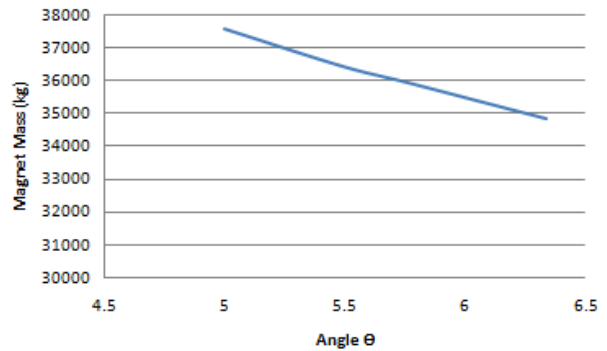**Figure 11:**Flux density vs. θ for a ferrite magnet rotor with angular pole.

Figure 12: Magnet mass vs. angle θ. All points on the curve give the same fundamental airgap flux density.

The results of the generator modelling is shown in Table 4 and the efficiencies are shown in Figure 13. This shows that the example generator with surface mounted NdFeB studied here is marginally more efficient than its ferrite counterpart (at and above rated wind speed).
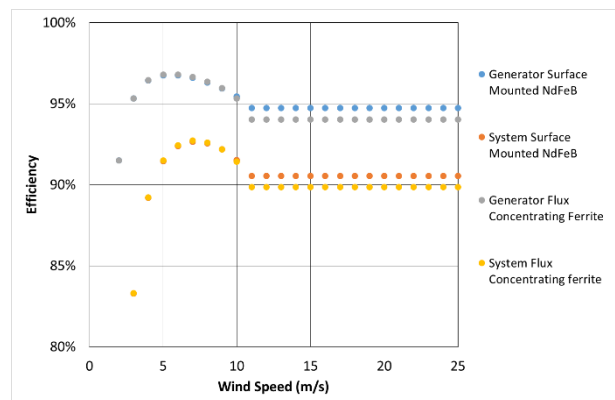

Figure 13: Generator and system efficiency curves for surface mounted NdFeB generator and flux concentrating ferrite generator

Table 4: Generator Dimensions and Parameters

	Surface Mount NdFeB	Flux Concentrating Ferrite
Generator Dimensions		
Stator radius, r_s (m)	3.5	3.5
Stack length,	1.5	1.5
Number of pole pairs	100	100
Air gap g (mm)	7	7
Stator slot width w_s (mm)	18.33	18.33
Stator tooth width w_t (mm)	18.33	18.33
Stator slot height h_s (mm)	80	80
Stator yoke height h_{sy} (mm)	40	40
Rotor yoke height h_{ry} (mm)	40	40
Pole width w_p (mm)	82	82
Magnet height h_m (mm)	15	400
Al ring height h_{al} (mm)	-	100
Generator Parameters		
Main inductance per phase L_{mph} (mH)	4.4	11.8
Direct axis inductance per phase L_d (mH)	48.3	59.3
Quadrature axis inductance per phase L_q (mH)	48.3	64.4
Stator resistance R_s (mΩ)	600	600
Generator Material Weight (tonne)		
Iron	31.4	66.2
Copper	8.1	8.1
Magnet	2.8	37.6
Total	42.3	119.6
Inertia (kg.m^2)		
Generator rotor inertia	156783	898587

3.2 Impact of inertia

The added inertia due to the extra mass on the flux concentrating ferrite generator rotor does not appear to make a significant change to the energy capture of the turbine. Figure 14 shows the power output for different generator rotor inertias when the mean wind speed is 10m/s. Even when the generator inertia is double that of the flux concentrating ferrite machine, the change in energy capture are only modest. This is probably due to the fact that the drivetrain inertia is 2 orders of magnitude smaller than the wind turbine rotor. Figure 15 shows the ratio energy captured between that of the two generator rotor inertias. This small effect was added with the generator efficiency and assumed availability to calculate the annual energy yield in Table 5.
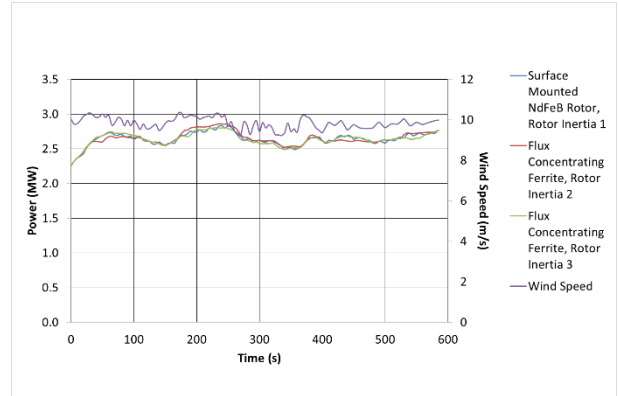

Figure 14: Power production against time for different generator rotor inertias. Rotor Inertia 1 = 157×10^3kgm^3; Rotor Inertia 2 = 899×10^3kgm^3; Rotor Inertia 3 = 2×Rotor Inertia 2.
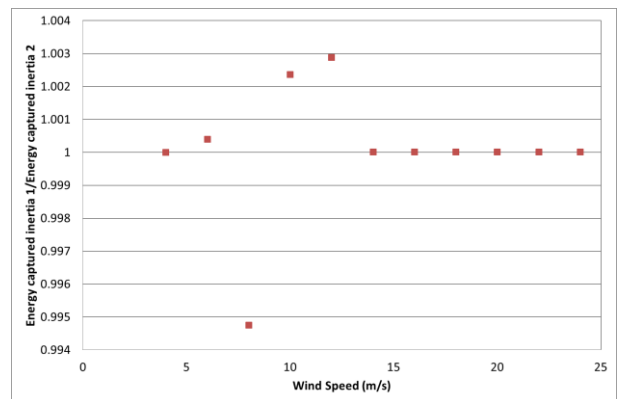

Figure 15: Ratio of sample energy capture with different generator rotor inertia

Table 5: Annual Energy Yield, Annual Losses and Cost of Energy of both generators.

Annual Energy		
	Surface Mount NdFeB	Flux Concentrating Ferrite
Joule losses (MWh)	1340	1489
Iron losses (MWh)	225	222
Converter and transformer losses (MWh)	1329	1329
Total losses (MWh)	2894	3041
Energy yield (GWh)	27.8	27.6
Cost of Energy		
ICC inc. BOP (kEuro)	21386	21399
AOM (kEuro)	628	628
FCR	0.116	0.116
COE (Euro/MWh)	111.8	112.6

3.3 Cost of energy

Table 5 shows that the flux concentrating Ferrite generator modelled here costs more than the surface mounted NdFeB generator. Because of

this and its lower efficiency (and hence lower energy yield) the Cost of Energy is higher.

Considering that the cost of NdFeB magnets is variable, it is possible to see what cost would lead to a breakeven level of Cost of Energy. For these example designs of the two types of generators, when the cost of NdFeB is €135/kg or more then the flux concentrating Ferrite machine will give better (i.e. lower) Cost of Energy.

As the generators presented here are examples, but not optimized generators, it is possible that the flux concentrating generator's energy yield could be improved so that it is equal to the surface mounted NdFeB generator. If this were the case (and costs are assumed to be constant as in Table 5), then the Cost of Energy of the two generator systems would be equal when the cost of NdFeB magnets increases to €65/kg.

4 Conclusion

This paper presented two generators with the same stator design but different rotors, one using NdFeB magnets in a surface mounted configuration and one with flux concentrating Ferrite magnets. These were designed and modelled for a 6MW offshore wind turbine.

The generators were compared in terms of energy yield with electrical and magnetic models. The effect of the increased inertia on turbine energy capture was assessed through time series turbine modelling, but it was found that this did not have a major impact on annual energy yield calculations.

In terms of Cost of Energy, the two generators gave similar results but the one with NdFeB magnets is generally better. If the flux concentrating Ferrite magnet generator's efficiency be improved (through optimization) or should the cost of NdFeB increase significantly then the Cost of Energy of the Ferrite machine will be lower than that of the turbines with NdFeB.

The closeness of the results suggest that these generators are worth investigating further for future scenarios where NdFeB magnet prices may increase or have increased uncertainty.

5 References

[1]C. Hurst. (2010, March). China's Rare Earth Elements Industry: WhatCan the West Learn?. Institute for the Analysis of Global Security(IAGS), U.S. Army's Foreign Military Studies Office, Fort Leavenworth, KS. [Online]. [Cited 7/3/15] Available at:http://www.iags.org/rareearth0310hurst.pdf

[2] Spooner, E., and A. C. Williamson. "Direct coupled, permanent magnet generators for wind turbine applications." *IEE Proceedings-Electric Power Applications* 143.1 (1996): 1-8.

[3] S. Eriksson and H. Bernhoff, "Rotor design for PM generators reflecting the unstable neodymium price," in *Electrical Machines (ICEM), 2012 XXth International Conference on*, 2012, pp. 1419-1423.

[4] K. Hart, A. McDonald, H. Polinder, E. Corr, and J. Carroll, "Improved cost of energy comparison of permanent magnet generator for large offshore wind turbines", *EWEA annual conference*,Barcelona, 2014.

[5] Introduction to NdFeB magnets. [Online]/ [Cited 7/3/15] Available at: http://www.ndfeb-info.com/

[6] J. Carroll, A. McDonald, J. Feuchtwang, D. McMillan, "Drive Train Availability in Offshore Wind Turbines"*EWEA annual conference*, Barcelona, 2014.

[7] Finite Element Method Magnetics software. Available at: http://www.femm.info/wiki/HomePage

[8]S. Eriksson, "Inherent Difference in Saliency for Generators with Different PM Materials," Journal of Renewable Energy, vol. 2014, Article ID 567896, 5 pages, 2014. doi:10.1155/2014/567896

[9]J. Pyrhonen, T. Jokinen, V. Hrabovcova,"Design of Rotating Electrical Machines," *Wiley* 2009;pp 230-249, 527-529.

[10] H. Polinder, F. Van der Pijl, G-J. De Vilder, and P.J. Tavner. "Comparison of direct-drive and geared generator concepts for wind turbines."*Energy conversion, IEEE transactions on* 21, no. 3 (2006): 725-733.

[11] Bladed Wind turbine simulation tool. Details available at: https://www.dnvgl.com/services/bladed-3775